A Novel Thermal Analysis Method of Tubular PM Linear Motors Based on Transfer-Learning

Tao Wu, *Member IEEE*, Peipei Dai, Youguang Guo, *Senior Member, IEEE,* Gang Lei, *Senior Member, IEEE,* Jianguo Zhu, *Senior Member, IEEE,* and Yifei Wang

***Abstract*—**Thermal modeling and analysis are critical for permanent magnet linear synchronous motors (PMLSMs), particularly in multi-physical analysis and motor design optimization. This paper proposes a new method for thermal steady state modeling and analysis based on transfer learning, which combines the thermal mechanism model with the data-driven model to achieve high-precision temperature analysis with small number of finite element analysis (FEA) samples.

First, an equivalent thermal circuit (ETC) model is established for the PMLSMs based on the structural parameters and heat transfer principles. Second, a hybrid model based on transfer learning is developed: the model is pre-trained by a large sample set generated from the ETC in the source field (mechanism analytical model), and then the trained model is transferred to the target field (FEA data-driven model). The parameters of the neural network in the target field are optimized by a few FEA sample sets with higher precision to improve the prediction accuracy of the target model.

Experimental results demonstrate that the proposed method significantly boosts the performance of the deep neural network (DNN) model, particularly when training sets are small. The root mean square error (RMSE) of the DNN model decreases by 0.901 in the 5:5 (training/testing) dataset and 1.726 in the 2:8 dataset; and the corresponding R^2 and maximal absolute error of motor performances are significantly decreased. The smaller the proportion of the training set, the better performance of the hybrid modeling will achieve. Furthermore, a temperature rise experiment conducted on a prototype motor validates the efficacy and precision of the proposed hybrid modeling methodology.

***Index Terms*—Deep neural network, Equivalent thermal circuit, Thermal modeling, Transfer learning, Hybrid model, Permanent magnet linear synchronous motor**

Manuscript received Month x, 2024; revised Month xx, 2024; accepted Month x, 2024. The work is supported in part by the Natural Science Foundation Project of China under Grant 61703376. (Corresponding author: Youguang Guo)

T. Wu, P. Dai, and Y. Wang are with the School of Automation, China University of Geosciences, Wuhan 430074, China, and also with the Hubei Key Laboratory of Advanced Control and intelligent Automation for Complex Systems, Wuhan 430074, China (e-mails: wutao@cug.edu.cn; Daisypp@cug.edu.cn; 1202011318@cug.edu.cn).

Y. Guo and G. Lei are with the School of Electrical and Data Engineering, University of Technology Sydney, NSW 2007, Australia (e-mails: youguang.guo-1@uts.edu.au; gang.lei@uts.edu.au).

J. Zhu is with the School of Electrical and Computer Engineering, University of Sydney, Sydney, NSW 2006, Australia (e-mail: jianguo.zhu@sydney.edu.au).

.

I. Introduction

A. Background and Motivation

Permanent magnet (PM) linear synchronous motors (PMLSMs) are extensively utilized across various sectors, such as industry, transportation and the medical field, owing to their streamlined structural design and proficient linear motion capabilities. As the imperative for elevated power density in motor design escalates, the significance of thermal analysis has correspondingly risen. The quest for optimal motor performance is marked by the inherent trade-off between achieving maximum power density and maintaining thermal equilibrium, a central dilemma in the motor's optimization process. Furthermore, the unique, enclosed architecture characteristic of tubular PMLSMs can engender excessively high local temperatures coupled with inadequate heat dissipation properties. Such conditions may precipitate irreversible demagnetization of the motor's permanent magnets, subsequently negatively affecting the motor's operational efficiency and overall service life [1]. Therefore, thermal analysis for PMLSMs is crucial to provide essential data to improve the motor's performance and durability.

The equivalent thermal circuit (ETC) method [2] and finite element analysis (FEA) method [3] are currently the two most commonly used methods for thermal field analysis of the PMLSMs. The ETC method, predicated on the principles of heat transfer and circuit theory, has been formulated to serve as a thermal circuit mechanism model analysis tool [4]. It can finely emulate the changes in temperature rise of the motor's thermal field, while maintaining high computational efficiency. However, it suffers from inadequate computational accuracy and the inability to fully model the complex nonlinear thermal field variations in practical situations.

FEA is applicable to different structures and dimensions of motor thermal fields due to its capacity to address intricate nonlinear parameter coupling, nonlinear boundaries, and other nonlinear issues and its high computational accuracy. However, this method has drawbacks, such as high computational complexity and long computation time, making it difficult to apply to motor modeling and optimization [5][6].

Due to the limitations of ETC and FEA, some data-driven modeling methods that have the advantages of fitting real input-output mapping [7] have gradually become a new approach to solve the thermal modeling problem of PMLSM when the above-mentioned methods are difficult to meet the analysis

requirements. Common data-driven modeling methods include the support vector machines (SVM) [8], random forest (RF) [9] , deep neural network (DNN) [10] and Bayesian neural network [11]. However, data-driven models usually require a large amount of data for training, and in the case of insufficient training samples, overfitting and other problems are prone to occur [12].

To sum up, the ETC has short calculation time, but it has limited accuracy compared to the real data. The FEA has high accuracy, but its calculation time is long. With the increase of design variables, a large number of FEA samples may be needed, which may be a challenging task to complete. How to achieve an efficient and high-precision thermal model using only limited data has become an urgent research hot spot.

This paper proposes a new hybrid method for thermal modeling based on machine learning with small-size samples, which organically combines the thermal mechanism model with the data-driven model. The hybrid model artfully utilizes transfer learning as a tool to integrate the mechanism model (ETC) and the data-driven model based on high-accuracy FEA together, thereby improving the performance of the data-driven model and achieving accurate results even with small sample training sets.

Transfer learning can help model learn data characteristics in the target domain by using knowledge in the source domain [13], and improve the model's ability to recognize a few categories by balancing data of different categories, thus improving the model's generalization ability and interpretability [14]. Transfer learning is a way to integrate the physical model (ETC) and the data-driven model (DNN based on FEA data set). In essence, the strategic amalgamation of transfer learning with traditional machine learning and deep learning frameworks can provide innovative solutions to several existing model intricacies [15]. The pre-training knowledge is derived from thermal physical field models, a simple ETC model with poor accuracy. Only a small amount of FEA data are used to optimize the pre-trained DNN model and help improve the accuracy of the model. The comparative experimental results showed that this method could significantly improve the performance.

B. Contributions

There are three main contributions of this paper:

1) An equivalent thermal path mechanism model is established for tubular PMLSM based on the structural parameters and heat transfer principles.

2) A data-driven modeling approach based on DNN is presented to tackle the low accuracy of conventional mechanistic models and provide a self-learning model structure for transfer learning.

3) A hybrid modeling method based on transfer learning is proposed, which significantly improves the model performance of the neural network on the small sample training set, and solves the long calculation time of FEA and the large amount of data required in high dimensional models in the practical applications.

II. Motor Structure and Thermal Analysis

A. Motor Structure

The schematic diagram of PMLSM structure is shown in Fig. 1, where $2b$ represents the length of the annular permanent magnet, τ_p represents the pole pitch, τ_{wp} represents the axial distance of the coil, and $\tau_p = \tau_{wp}$, τ_w represents the axial width of the single-phase coil, R_{s1} represents the outer radius of the moverstator, R_{s2} represents the inner radius of the moverstator, R_{m1} represents the outer radius of the stator PMs, and R_{m2} represents the inner radius of the PMs. The size parameters of the main parts of PMLSM are listed in Table I.

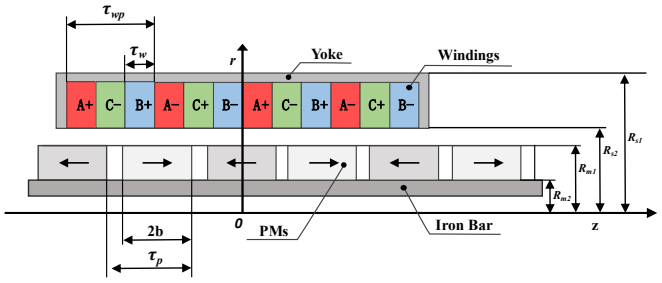

Fig. 1. Parametric structure diagram of PMLSM.

TABLE I
Main Parts Dimensional Parameters of the PMLSM

Quantity	Symbol	Value	Unit
Outer radius of mover	R_{s1}	33	mm
Inner radius of mover	R_{s2}	18	mm
Outer radius of PM (Stator)	R_{m1}	17	mm
Inner radius of PM (Stator)	R_{m2}	9	mm
Air gap length	Σ_s	1	mm
Pole pitch	τ_p	36	mm
Total length of mover	L_m	900	mm

B. Finite Element Analysis Method

The FEA method based on the variational principle has been widely used in the quantitative analysis and optimal design of motor thermal field thanks to its universal applicability. It is considered as a reliable and approximately realistic source of data [16].

The process of building the PMLSM FEA thermal model in this paper is as follows. Firstly, the geometric model of the motor is built in ANSYS according to the dimensional parameters of PMLSM shown in the previous section. Secondly, the software automatically generates the meshes according to the geometrical structure characteristics of the motor model; Finally, the losses in the various parts of the motor are added to the motor model in the form of load [17]. After setting the relevant parameters, the thermal process is simulated by varying the values of copper loss ranging from 100 to 1500 W, iron loss from 20 to 300 W, and PM eddy current loss from 10 to 200 W [6]. The copper loss of the coil is evenly distributed to each coil, the eddy current loss of the PM is concentrated at the ends of the PMLSM [18], and the iron loss is evenly distributed in the iron yoke. The range of thermal parameters is determined based on the range of motor design variables, as stated in our previous article [19]. While keeping other conditions constant, the steady temperatures of the core, coil, and PM are recorded, generating a total of 540 simulation sets. Fig. 2 displays the motor's temperature rise model.

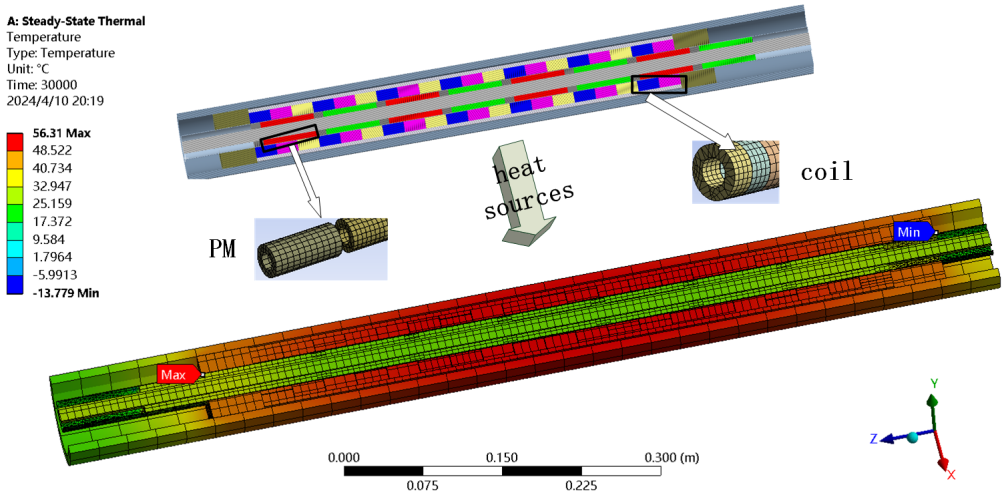

Fig. 2. Structure and temperature rise diagram of PMLSM.

C. Equivalent Thermal Circuit Method

FEA has the capability to predict the temperature distribution of a motor with high accuracy, but the complexity of its analysis process generates limited data, and demands an enormous amount of computational resources. The ETC method offers a straightforward modeling process and rapid calculation, allowing extensive data output generation. This feature permits swift evaluation of the temperature distribution within the motor. It is, therefore, possible to achieve more efficient motor design and optimization through the integration of FEA and ETC models in the analysis of the thermal field of PMLSM.

In this paper, the ETC method is used to establish a thermal field mechanism model for the PMLSM. Based on Simulink, a complete motor thermal circuit model is constructed by building each equivalent element of the motor. The loss generated by the motor operation constitutes the heat source in the thermal circuit, and the distributed heat source inside the motor is regarded as a certain point. Based on this, the heat conduction of each structure and the heat dissipation effect of each surface can be reflected by the equivalent thermal resistance. The complete thermal circuit structure diagram is illustrated in Fig. 3.

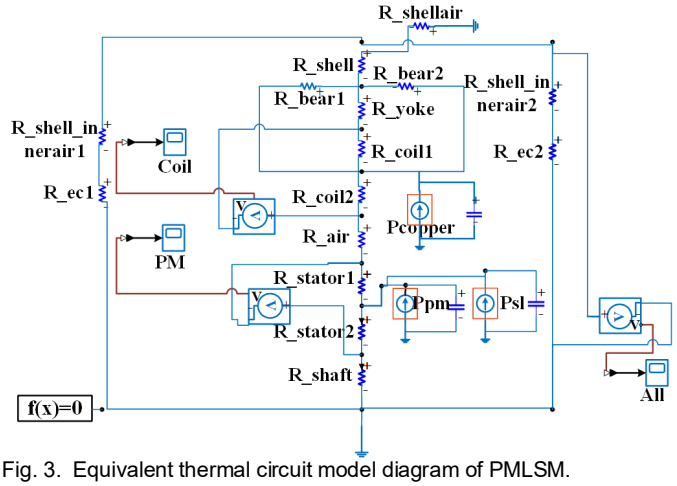

Fig. 3. Equivalent thermal circuit model diagram of PMLSM.

The resistor in the figure represents the thermal resistance of the corresponding part of the motor, the capacitor represents the thermal capacity of the corresponding part, and the DC current source represents the loss of the corresponding part. By solving the circuit in Simulink and acquiring the voltage at each node, the temperature rise of the motor part corresponding to the node can be obtained, and according to the range of values of copper loss, iron loss and PM eddy current loss, the temperature rise data of 540 groups are obtained.

The ETC model is capable of fitting the temperature rise of PMLSM, but its computational accuracy is significantly lower than that of non-linear FEA models, owing to its linear computational process. Even though ETC dataset is not directly suitable for training data-driven models, it aptly incorporates the data attributes of the thermal field of the PMLSM. Also, owing to its high volume and rapid generation capabilities, the dataset is appropriate for transfer learning to pre-train.

III. Hybrid Modeling Method

A. Model Structure of Deep Neural Network

The accuracy of the ETC mechanism model is low, and the predicted results may have significant deviation from the actual temperature rises. Aiming at this issue, a DNN model based on the FEA dataset is established in this paper. The DNN model has better learning ability in high dimensional and transfer learning than conventional machine learning and shallow neural network models. DNN is a deep learning model based on neurons that builds a multi-layer network structure, which can be used for various prediction and classification tasks. It gradually extracts the feature representation of the input data through a large amount of training data and multi-layer nonlinear transformation and finally realizes tasks such as classification or regression of the data.

After optimization of all parameters, the structure of the DNN model used in this paper is shown in Fig. 4, which consists of one input layer, two fully connected linear layers and one output layer. The optimal number of linear layer neurons is determined after repeated experiments. The input layer contains the three loss values (copper loss, iron loss, and PM eddy current loss), and the data is normalized using the BatchNorm1d function. To capture complex patterns and

relationships in the input data, the first linear layer is a fully connected layer with 24 neurons, the output of which is fed to the second linear layer with 12 neurons after the ReLU activation function, and then to the output layer with 3 neurons after the ReLU. The ReLU activation function can introduce nonlinearities that allow the model to learn more complex functions. Finally, the temperature rise values of the three parts (overall temperature rise, coil temperature rise, and PM temperature rise) are the output. It should be noted that as the data are always definite in the data-driven model, the dynamic changes of copper loss with temperature rising is hard to handle. Hence, multiple iterations are used to calculate the temperature rise through the steady state TL-DNN model. Firstly, input the initial copper loss data, calculate the temperature rising, and then update the new copper loss as input into the TL-DNN model, until the temperature rise error is less than the set threshold.

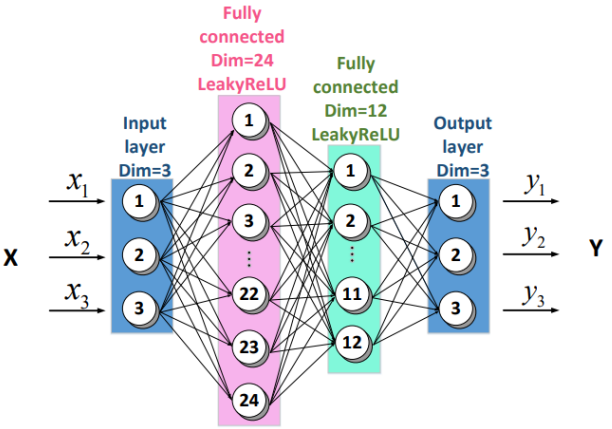

Fig. 4. Structure diagram of DNN model.

The model uses Adam optimization algorithm, the initial learning rate is set to 0.001, and the LambdaLR function is used to update the learning rate automatically during the model training. With 30 samples as a batch, 20 epochs are trained in each round, and the training period is 150 rounds.

B. Evaluation of Thermal Field Model

To validate the accuracy of the DNN model, the root mean square error (RMSE), mean absolute error (MAE) and correlation coefficient (R^2) are selected as the evaluation metrics for model training accuracy and generalization performance. Due to the existence of multiple feature indicators and label values in the thermal field of PMLSM, this paper has established a 3-input, 3-output model with copper, iron and PM eddy current losses as the inputs, and the overall motor temperature rise, coil temperature rise and PM temperature rise as the outputs.

RMSE is a typical metric for regression models, used to indicate the magnitude of the model's errors in prediction, with higher weight placed on larger errors. Its calculation formula is as follows:

$$RMSE = \sqrt{\frac{1}{nm}\sum_{i=1}^{n}\sum_{j=1}^{m}(y_{ij}-\hat{y}_{ij})^2} \tag{1}$$

MAE is used to measure the unbiasedness of a model, as it can avoid the mutual offset of errors and accurately reflect the actual prediction error. Its calculation formula is as follows:

$$MAE = \frac{1}{nm}\sum_{i=1}^{n}\sum_{j=1}^{m}|\, y_{ij}-\hat{y}_{ij}\,| \tag{2}$$

R^2 is used to evaluate the fitting degree of the model to the true values, and its calculation formula is:

$$R^2 = 1-\frac{\sum_{i=1}^{n}\sum_{j=1}^{m}(y_{ij}-\hat{y}_{ij})^2}{\sum_{i=1}^{n}\sum_{j=1}^{m}(y_{ij}-\overline{y}_{j})^2} \tag{3}$$

In (1), (2) and (3), n represents the number of samples for the whole thermal field, m is the number of labels, $\hat{y}_{ij}$ is the predicted value of the jth label of the ith sample, y_{ij} is the true value of the jth label of the ith sample, and $\bar{y}_j$ is the mean value of the jth label.

C. Prediction Results and Analysis

In order to validate the accuracy of the DNN model, this study has put 540 sets of FEA data into training and testing sets according to the ratio of 8:2. The prediction results of the DNN model are compared with other data-driven models, including support vector machine (SVM), random forest (RF) and shallow neural network model extreme learning machine (ELM).

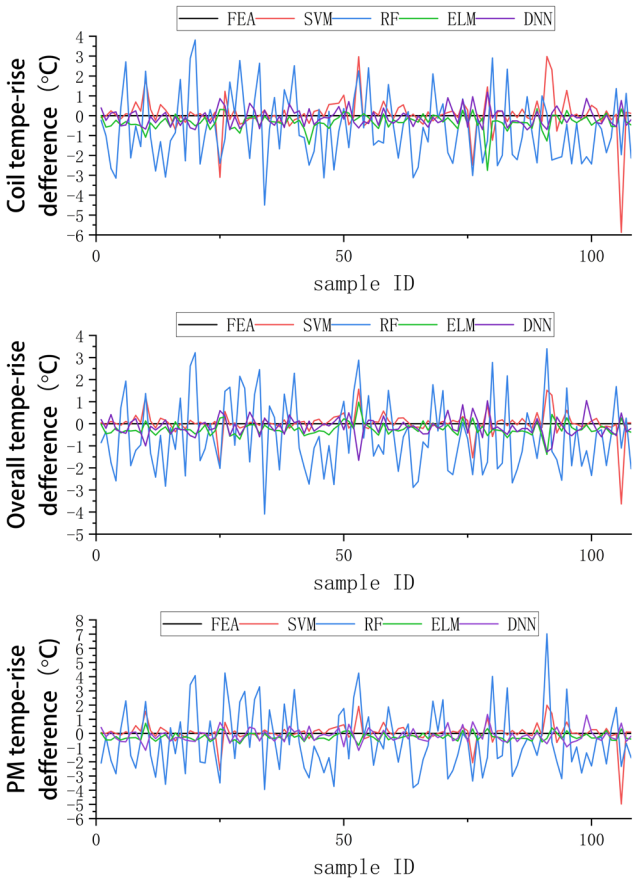

Fig. 5. Differences among temperature rise of four models and FEA.

Additionally, to ensure fairness, the ELM's layer structure, parameters, optimization algorithm, and training iterations are kept consistent with the DNN.

Fig. 5 compares the performance of four PMLSM data-driven models. As shown, the temperature rise predicted by the DNN is the closest to the FEA data, compared with the temperature rises predicted by the RF, SVM and ELM.

In addition, to demonstrate the superiority of the data-driven model clearly, the values of RMSE, MAE and R^2 are obtained separately for each method on the test set using 10-fold cross-validation. The results are listed in Table II.

TABLE II
COMPARISON OF PERFORMANCE OF DATA-DRIVEN MODELS UNDER 10-FOLD

	RMSE	MAE	R^2
RF	1.939	1.513	0.9976(0.0034)
SVM	1.887	1.401	0.9977(0.0033
ELM	1.252	0.727	0.9982(0.0018)
DNN	0.974	0.617	0.9997(0.0003)
ETC	17.36	10.57	0.7668(0.2332)

From Table II, it can be seen that:

1) The RMSE, MAE, and R^2 of conventional machine learning models in the multiple-input and output motor temperature rise dataset are inferior to the neural network model, indicating that the neural network model better fits the high-dimensional nonlinear data.
2) The RMSE, MAE, and R^2 of the DNN model are better than those of the ELM model, indicating that the generalization ability and robustness of the DNN are higher than those of the shallow neural network.
3) The accuracy of ETC model is quite poor. The RMSE, MAE, and R^2 of the four data-driven models are much better than those of the ETC mechanism model, which verifies the accuracy and superiority of the data-driven model by the FEA dataset.

The conclusions in this section are based on the premise that FEA can provide sufficient training samples. In practical applications, real-time monitoring and prediction of motor operating conditions are often required, but the computationally intensive and time-consuming nature of FEA usually does not allow sufficient data to be generated in actual projects. On the one hand, a sufficient FEA requires designers to spend a lot of time. On the other hand, as the dimension (n) of variables increases, e.g. taking 5 sets for each variable requires at least 5^n sample data. This huge sample is an almost impossible task to achieve. When the FEA data is insufficient, the data-driven model cannot be adequately trained, which may lead to the degradation of model function, generalization ability, and underfitting or overfitting phenomena.

Therefore, further research is needed on combining the FEA, ETC mechanism model, and data-driven model to solve the problems mentioned above.

D. Hybrid Modeling Process

Transfer learning can transfer the feature knowledge that has been learned to a new task and improve the learning effect and generalization ability of the new task. Meanwhile, DNNs have advantages in hidden layer representation learning, multi-level feature extraction and structural similarity [20]. Therefore, compared with conventional machine learning algorithms, transfer learning is more suitable for the training of DNN models [21].

Among the two thermal field analysis methods, the ETC mechanism model is easy to generate a large amount of data, which can help the data-driven model to better learn the distribution characteristics of the data and improve the generalization ability of the model, so the data of ETC is used as the source domain data set. The data generated by the FEA model is less but with high accuracy, which can well reflect the data characteristics of the actual temperature rise, so the data of FEA is used as the target domain data set. The PMLSM thermal field hybrid modeling process is shown in Fig. 6.

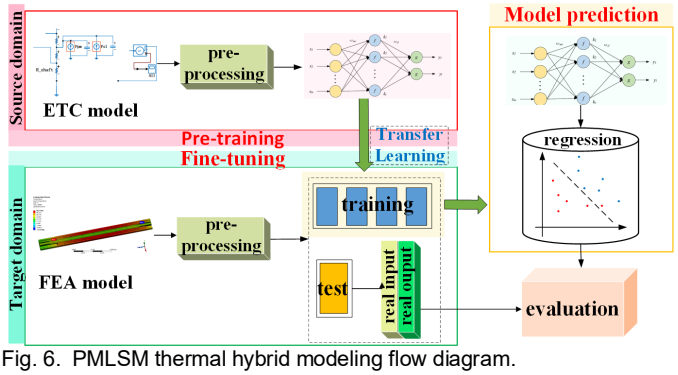

Fig. 6. PMLSM thermal hybrid modeling flow diagram.

The following are the specific steps:

1) Data preprocessing is performed on the ETC dataset to obtain the pre-training sample set A, and simultaneously on the FEA dataset to obtain the training sample set B and the test sample set B.
2) The sample set A is substituted into the source domain to pre-train the data-driven model.
3) The pre-trained data-driven model is transferred to the target domain based on the training sample set B for secondary training with parameter fine-tuning to keep the model parameters updated.
4) After secondary training, the predicted temperature rise output values are obtained by substituting the test sample set B into the data-driven model.

The predicted temperature rise values of the target domain are compared with the actual temperature rise values in the test sample set B and evaluated.

IV. RESULTS AND DISCUSSION

A. Pre-training

The purpose of pre-training is to let the model fit the ETC dataset to characterize as many data properties of the PMLSM thermal field as possible. Therefore, all the 540 sets of ETC data are directly used as pre-trained sample sets, and the four data-driven models, RF, SVM, ELM, and DNN, are pre-trained, respectively. The pre-training results are shown in Fig. 7.

Since the ETC model is essentially a linear model, the relationship between the input and output data is linear, and the pre-training stage does not separate the data into training and test sets. Therefore, all four data-driven models fit extremely well on the ETC sample set, with the DNN model fitting even

close to 100%. In addition, the RMSE, MAE and R^2 are calculated for each data-driven model on the ETC sample set after pre-training using 10-fold cross-validation. The results are shown in Table III.

TABLE III
COMPARISON OF PERFORMANCE OF DATA-DRIVEN MODELS UNDER 10-FOLD CROSS-VALIDATION

	RMSE	MAE	R^2
RF	0.572	0.264	0.9999
SVM	0.599	0.187	0.9999
ELM	0.059	0.048	0.9999
DNN	0.034	0.015	0.9999

The R^2 of all four data-driven models reached 0.9999, indicating that the models have fitted and interpreted the linear data very well. All the models have learned the data characteristics of the PMLSM thermal field well, laying the foundation for the next step of model transfer.

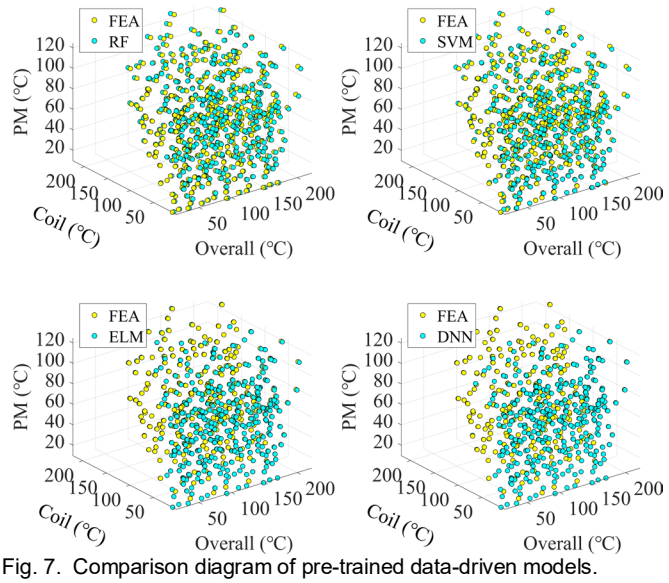

Fig. 7. Comparison diagram of pre-trained data-driven models.

B. Model Transfer and Parameter Fine-tuning

To verify the enhancement effect of transfer learning on data-driven models, as well as to validate the effect of transfer learning on small sample training sets and to test the performance of the models in the case of insufficient training sample sets, the 540 sets of FEA data are divided into training and testing sets in the ratios of 8:2, 5:5, and 2:8, respectively, and the four pre-trained data-driven models are substituted into the training sample sets of three different ratios in the target domain for secondary training with fine-tuned parameters. Meanwhile, the four data-driven models are also trained directly based on three different ratios of data sets, respectively, to compare the hybrid modeling approaches. To ensure fairness, the structure of each layer, parameters, optimization algorithms, number of training rounds and evaluation metrics of the models used in both modeling approaches are kept consistent. The results are shown in Figs. 8-10.

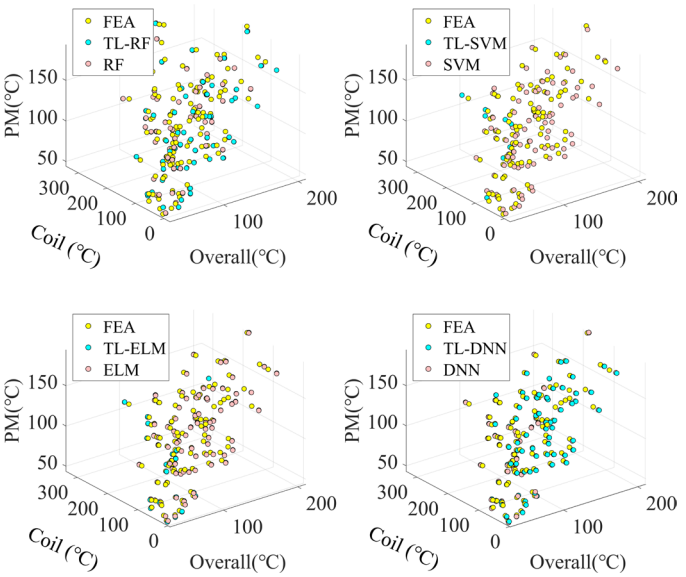

Fig. 8. Comparison diagram based on different modeling methods (8:2).

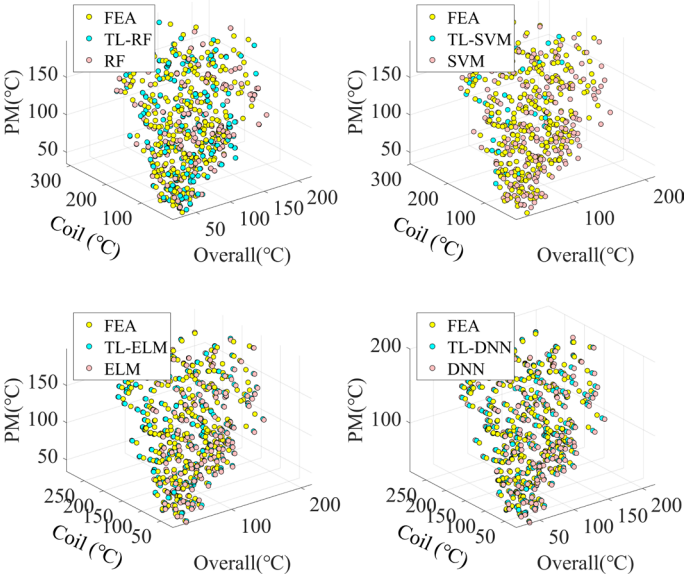

Fig. 9. Comparison diagram based on different modeling methods (5:5).

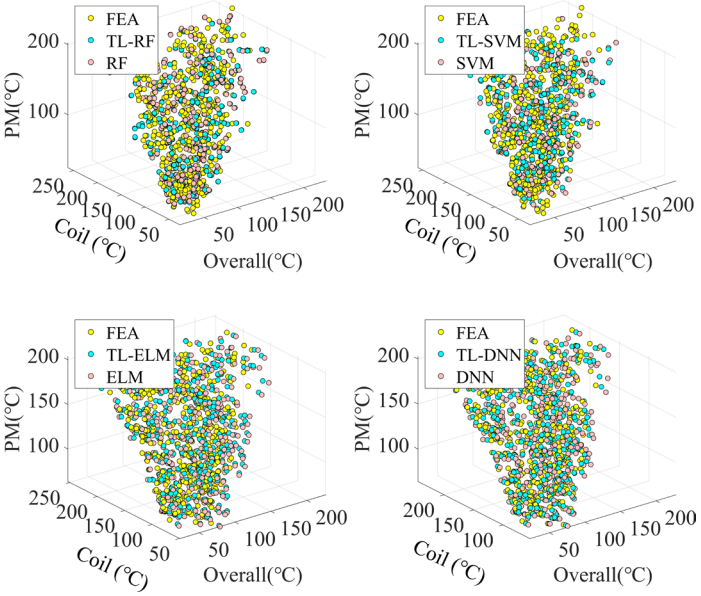

Fig. 10. Comparison diagram based on different modeling methods (2:8).

From the figures, it can be seen that the results of the hybrid modeling methods all outperform those of the direct modeling methods. Meanwhile, among the four data-driven models after transfer learning, the DNN model predicts the 3D motor temperature rise data better than the RF, SVM and ELM models, and it has the closest fit with the real data.

RMSE, MAE and R^2 are calculated for each data-driven model using 10-fold cross-validation on different proportions of the test set, and the results are tabulated in Tables IV and VI.

TABLE IV
PERFORMANCE EVALUATION OF DATA-DRIVEN MODELS (USING TRANSFER LEARNING)

		TL-DNN	TL-RF	TL-SVM	TL-ELM
RMSE	8:2	0.674	4.466	5.279	1.341
	5:5	1.488	4.701	6.499	1.554
	2:8	2.720	5.787	11.171	2.573
MAE	8:2	0.644	3.492	4.057	1.051
	5:5	0.526	3.717	4.890	0.568
	2:8	1.888	4.580	7.753	1.763
R^2	8:2	0.9997	0.991	0.985	0.9952
	5:5	0.9969	0.990	0.981	0.9966
	2:8	0.9943	0.984	0.941	0.9930

TABLE V
PERFORMANCE EVALUATION OF DATA-DRIVEN MODELS (WITHOUT TRANSFER LEARNING)

		DNN	RF	SVM	ELM
RMSE	8:2	0.487	4.931	5.167	1.408
	5:5	2.389	5.184	6.047	2.920
	2:8	4.446	7.360	12.277	5.989
MAE	8:2	0.341	2.565	1.931	1.088
	5:5	1.504	3.046	2.892	2.018
	2:8	2.531	5.146	8.433	3.794
R^2	8:2	0.9998	0.987	0.986	0.995
	5:5	0.9919	0.985	0.980	0.9870
	2:8	0.9869	0.969	0.915	0.9625

TABLE VI
COMPARISON OF MODEL PERFORMANCE EVALUATION

		DNN	TL-DNN	IMPROVEMENT
RMSE	8:2	0.487	0.674	-0.187
	5:5	2.389	1.488	0.901
	2:8	4.446	2.720	1.726
R^2	8:2	0.9998	0.9997	-0.0001
	5:5	0.9919	0.9969	1.0005
	2:8	0.9869	0.9943	1.0007
$\|1-R^2\|$	8:2	0.0002	0.0003	-50%
	5:5	0.0081	0.0031	61.73%
	2:8	0.0131	0.0057	56.49%

Based on the results listed in Tables III to VI, the following conclusions can be drawn:

1) On all three ratios of the dataset, transfer learning (TL) has a non-significant or even negligible enhancement effect on the RF model and does not have any enhancement effect on the SVM model.
2) In contrast, the fits of the TL-ELM model and the TL-DNN model are significantly better than that of the conventional machine learning model on all three scaled datasets, while the TL-DNN outperforms the shallow neural network model TL-ELM.
3) With sufficient data in the training set, the DNN model fits slightly better than the TL-DNN model, with RMSEs of 0.487 and 0.673, respectively. This is due to the fact that TL uses a pre-training dataset with some errors, which may dilute the model's fit to the real data and affect its accuracy when there are large errors in the pre-training dataset.
4) According to the data analysis, when the training sample of ELM model is reduced from 8:2 to 2:8, the change of the RMSE before and after using transfer learning increases from 0.067 to 3.416. Similarly, the reduction of RMSE by transfer learning increases from -0.187 to 1.726 when the training sample of the DNN model is reduced from 8:2 to 2:8. The above-mentioned data comparison illustrates that in transfer learning the smaller the training sample set of the target task, the better the improvement effect of transfer learning tends to be.

As the training sample decreases, e.g. the ratio of training set to prediction set is reduced from 8:2 to 2:8, the improvement effect of transfer learning on the model gradually increases. The advantages of migration learning come to the fore when the amount of data in the training set is no longer sufficient to adequately train the model and, at the same time, the size of the test set to be fitted is still increasing. After pre-training with the ETC dataset, the TL-ELM model and TL-DNN model still perform relatively well in fitting the features of the training set with small-scale real data. Further, it indicates that transfer learning can greatly improve the generalization ability of neural network models in small sample datasets. Moreover, since the ETC dataset has a certain amount of error noise, pre-training with noisy datasets allows the model to learn richer features, which makes the model more capable to cope with various noises and disturbances in the target domain, thus greatly improving the robustness of the model in small sample datasets.

V. EXPERIMENTS AND COMPARISON

In order to verify the accuracy of the TL-DNN model, the temperature rise experiments on a prototype are carried out. A PMLSM and its oscillatory motion platform are established as shown in Fig. 11. The actuator (Copley Xenus XSJ-230-10) adopted the current control mode (current tracking control mode), and the given current is an oscillating square wave with amplitude i_q =4A. The oscillatory stroke is 200 mm and the current is set as i_q =4 A as shown in Fig. 12 and the amplitude of phase alternating current is about I_m=4.2A. The phase resistance of the winding is R=9 Ω so the copper loss of the PMLSM is calculated as:

$$P_{cua} = 3I^2R = \frac{3}{2} I_m^2 R = 238.14W \tag{4}$$

Fig. 12 shows the square wave oscillation of the measured current when the reference current i_q=4A. Fig. 13 shows the speed curve under a 200 mm oscillating stroke. All these data can be directly recorded by the computer control software. When i_q = 4 A, the PM eddy current loss P_{eddy} is approximately 5W according to the calculation method in [22], and the iron loss P_{iron} is 25 W measured by Watt meter (Total loss minus copper loss and PM eddy current loss). Another experiment condition is i_q=5 A, P_{cu} = 372.09W, P_{eddy} =7.4 W and P_{iron} = 39.8 W.

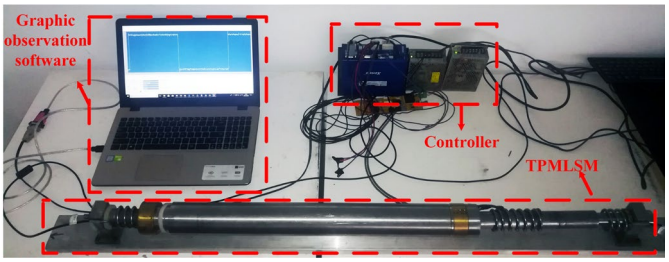

Fig. 11. Prototype and temperature rise measurement platform.

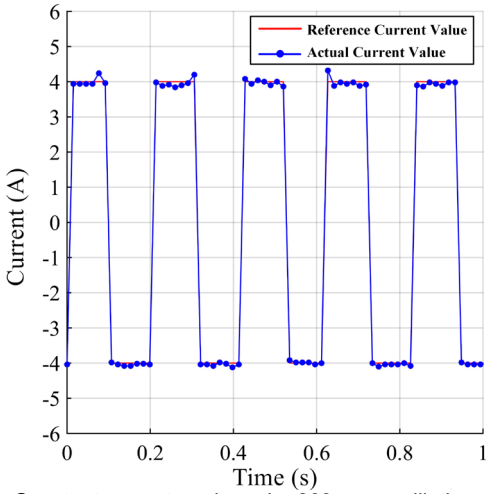

Fig. 12. Constant current mode under 200 mm oscillating stroke.

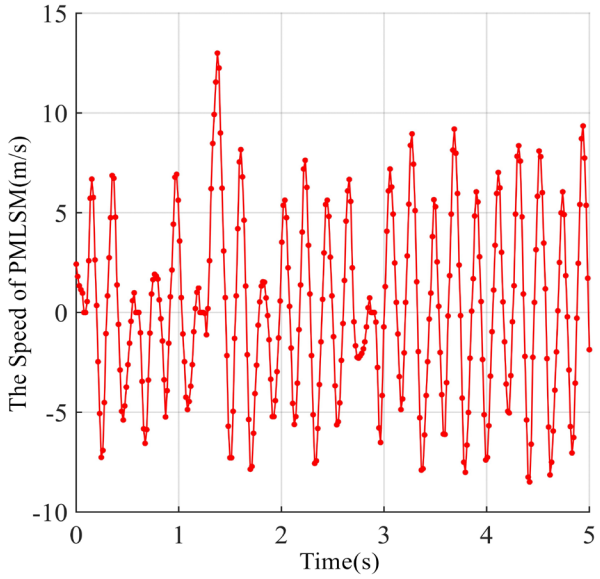

Fig. 13. The speed curve under 200 mm oscillating stroke.

The laboratory room temperature is maintained at 23℃. After two hours of continuous operation, the temperature curve along the surface of the PM measured with the infrared temperature gun is shown in Fig. 14.

The blue curve is the temperature curve when i_q =4 A with a 200 mm stroke, and the red curve is that when i_q =5 A with a 240 mm stroke. The average temperature rise of PM is calculated by taking the average value of the operation area. The measurement data shows that the highest temperature rise point of PM is close to the end of the mover, which is consistent with the simulation results of the eddy current calculation [22].

Another reason may be that the sliding friction losses are concentrated on these two ends. The average PM temperature rise from 100 mm to 1100 mm is about 54.8 ℃ in the blue curve, and the coil temperature rise is about 60.2 ℃ measured by the inner surface temperature at both ends of the mover. The temperature rise of the whole motor is marked with * for it is hard to estimate here, and the temperature of the inner coil cannot be measured under the experiment condition. In general, the predicted temperature rise data is in good agreement with the experimental data. The comparison between prediction results by TL-DNN and experimental results is shown in Table VII. The errors are below 2%.

TABLE VII
COMPARISON BETWEEN PREDICTION AND EXPERIMENTAL RESULTS

Motor parts	Overall temperature rise (℃)	Coil temperature rise (℃)	PM temperature rise (℃)
TL-DNN Predictions ($p_{cu} = 238.14W$)	50.97	60.65	55.79
Experimental results	*	60.2	54.8
Error	*	0.45(0.75%)	0.99(1.81%)
TL-DNN Predictions ($p_{cu} = 372.09W$)	61.18	74.66	67.55
Experimental results	*	73.3	67.1
Error	*	1.36(1.86%)	(0.45)0.67%

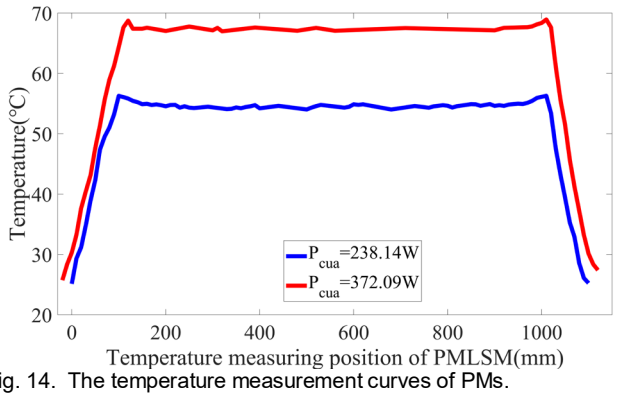

Fig. 14. The temperature measurement curves of PMs.

VI. CONCLUSION

This paper proposed a novel hybrid thermal model for tubular PMLSMs, which combined the ETC mechanism model with FEA-based DNN model. This approach can significantly improve the performance of DNN models with small sample training sets, avoiding the problem of FEA's long computation time, especially in high-dimensional models.

Multi-group training/test comparison experiments show that the higher prediction accuracy of the model was achieved when a lower training data ratio was used. Interestingly, while the training sample data is sufficient, the precision of the hybrid model unexpectedly has a downward trend, mainly because the ETC model has poor precision.

This hybrid driven model based on transfer learning might be an efficient and useful tool to solve thermal field problems. Although it is a steady state model, high-precision results can still be obtained through iterative calculations. It applies to electro-magnetic field analysis and may provide a new way for motor's multi-physical design and optimization in the future.

REFERENCES

[1] Z. Zhang, M. Luo, J. Duan, and B. Kou, "Design and modeling of a novel permanent magnet width modulation secondary for permanent magnet linear synchronous motor," *IEEE Trans. Ind. Electron.*, vol. 69, no. 3, pp. 2749-2758, Mar. 2022.

[2] Y. Guo, J. Zhu, and W. Wu, "Thermal analysis of SMC motors using a hybrid model with distributed heat sources," *IEEE Trans. Magn.,* vol. 41, no. 6, pp. 2124-2128, Jun. 2005.

[3] Y. Huang, J. Zhu, and Y. Guo, "Thermal analysis of high-speed SMC motor based on thermal network and 3-D FEA with rotational core loss included," *IEEE Trans. Magn.*, vol. 45, no. 10, pp. 4684-4687, Oct. 2009.

[4] H. Zhou, *et al.*, "Rapid prediction of magnetic and temperature field based on hybrid subdomain method and finite difference method for the interior permanent magnet synchronous motor," *IEEE Trans. Transport. Electrific.*, vol. 10, no. 3, pp. 6634-6651, Sep. 2024.

[5] Di Nardo, *et al.*, "Design optimization of a high-speed synchronous reluctance machine," *IEEE Trans. Ind. Appl.*, vol. 54, no. 1, pp. 233-243, Feb. 2018.

[6] T. Wu, Z. Feng, *et al.*, "Multi objective optimization of a tubular coreless LPMSM based on adaptive multi objective black hole algorithm," *IEEE Trans. Ind. Electron.*, vol. 67, no. 5, pp. 3901-3910, May 2020.

[7] X. Wang, Y. Wang, and T. Wu, "The review of electromagnetic field modeling methods for permanent-magnet linear motors," *Energies*, vol. 15, no. 10, article 3595, May 2022.

[8] F. Husari and J. Seshadrinath, "Incipient interturn fault detection and severity evaluation in electric drive system using hybrid HCNN-SVM based model," *IEEE Trans. Industr. Inform.*, vol. 18, no. 3, pp. 1823-1832, Mar. 2022.

[9] F. Xie, *et al.*, "The optimal speed-torque control of asynchronous motors for electric cars in the field-weakening region based on the RFR," *IEEE Trans. Ind. Electron.*, vol. 67, no. 11, pp. 9601-9612, Nov. 2020.

[10] L. Chen, *et al.*, "Noise-boosted convolutional neural network for edge-based motor fault diagnosis with limited samples," *IEEE Trans. Industr. Inform.*, vol. 19, no. 9, pp. 9491-9502, Sep. 2023.

[11] S. Liu, Z. Yang, Q. Wei, *et al.*, "Thermal error model of linear motor feed system based on Bayesian neural network," *IEEE Access*, vol. 9, pp.112561-112572, 2021.

[12] W. Kirchgässner, W. Oliver, and B. Joachim, "Data-driven permanent magnet temperature estimation in synchronous motors with supervised machine learning: a benchmark," *IEEE Trans. Energy Convers.*, vol. 36, no. 3, pp. 2059-2067, Sep. 2021.

[13] Y. Sun, K. Zhang, and C. Sun, "Model-based transfer reinforcement learning based on graphical model representations," *IEEE Trans. Neural Networks and Learning Systems*, vol. 34, no. 2, pp. 1035-1048, Feb. 2023.

[14] X. Yang, F. Li, and H. Liu, "TTL-IQA: Transitive transfer learning based no-reference image quality assessment," *IEEE Trans. Multimedia,* vol. 23, pp. 4326-4340, Dec. 2021.

[15] J. Asanuma, S. Doi, and H. Igarashi, "Transfer learning through deep learning: Application to topology optimization of electric motor," *IEEE Trans Magn.*, vol. 56, no. 3, pp. 1-4, Mar. 2020.

[16] Z. Xu, Y. Xu, Y. Gai, and W. Liu, "Thermal management of drive motor for transportation: analysis methods, key factors in thermal analysis, and cooling methods—a review," *IEEE Trans. Transport. Electrific.*, vol. 9, no. 3, pp. 4751-4774, Sep. 2023.

[17] J. Ryu, *et al.*, "Mathematical modeling of fast and accurate coupled electromagnetic-thermal analysis," *IEEE Trans. Ind. Appl.*, vol. 57, no. 5, pp. 4636-4645, Sep. 2021.

[18] J. G. Zhu, S. Y. R. Hui, and V. S. Ramsden, "A generalized dynamic circuit model of magnetic cores for low-and high-frequency applications. I. Theoretical calculation of the equivalent core loss resistance," *IEEE Trans. Power Electron.*, vol. 11, no. 2, pp. 246-250, Mar. 1996.

[19] J. G. Zhu, S. Y. R. Hui, and V. S. Ramsden, "A dynamic equivalent circuit model for solid magnetic cores for high switching frequency operations," *IEEE Trans. Power Electron.*, vol. 10, no. 6, pp. 791-795, Nov. 1993.

[20] X. Zhou, N. Zhai, S. Li, and H. Shi, "Time series prediction method of industrial process with limited data based on transfer learning," *IEEE Trans. Industr. Inform.*, vol. 24, no. 9, pp. 15853–15869, Aug. 2022.

[21] S. Park, *et al.*, "Deep transfer learning-based sizing method of permanent magnet synchronous motors considering axial leakage flux," *IEEE Trans. Magn.*, vol. 58, no. 9, pp. 1-5, Apr. 2020.

[22] T. Wu, *et al.*, "Calculation of eddy current loss in a tubular oscillatory LPMSM using computationally efficient FEA," *IEEE Trans. Ind. Electron.*, vol. 66, no. 8, pp. 6200-6209, Aug. 2019.